Peripheral astral microtubules ensure asymmetric furrow positioning in neural stem cells

Alexandre Thomas, Emmanuel Gallaud, Aude Pascal, Laurence Serre, Isabelle Arnal, Laurent Richard-Parpaillon, Matthew Scott Savoian, Régis Giet

Peripheral astral microtubules ensure asymmetric furrow positioning in neural stem cells

Running title: Peripheral astral microtubules recruit a dominant cortical pool of centralspindlin at the asymmetric division furrow

Alexandre Thomas[1], Emmanuel Gallaud[1], Aude Pascal[1], Laurence Serre[2], Isabelle Arnal[2], Laurent Richard-Parpaillon[1], Matthew Scott Savoian[3] and Régis Giet[1#].

[1.] Univ Rennes, CNRS, IGDR (Institut de Génétique et Développement de Rennes) - UMR 6290, F-35000 Rennes, France
[2.] Univ. Grenoble Alpes, Inserm U1216, CEA, CNRS, Grenoble Institut Neurosciences, GIN, 38000 Grenoble, France.
[3.] Massey University, School of Fundamental Sciences, 4410, Palmerston North, New Zealand

[#]. Corresponding author: regis.giet@univ-rennes1.fr

Lead Contact

Further information and requests for reagents generated in this study should be directed to and will be fulfilled by the Lead Contact, Régis Giet (regis.giet@univ-rennes1.fr).

Summary

Neuroblast division is characterized by asymmetric positioning of the cleavage furrow resulting in a large difference in size between the future daughter cells. In animal cells, furrow placement and assembly are governed by centralspindlin that accumulates at the equatorial cell cortex of the future cleavage site and at the spindle midzone. In neuroblasts, these two centralspindlin populations are spatially and temporally separated. A leading pool is located at the basal cleavage site and a second pool accumulates at the midzone before travelling to the cleavage site. The cortical centralspindlin population requires peripheral astral microtubules and the Chromosome Passenger Complex for efficient recruitment. Loss of this pool does not prevent cytokinesis but enhances centralspindlin signaling at the midzone leading to equatorial furrow repositioning and decreased size asymmetry. These data show that basal furrow positioning in neuroblasts results from a competition between different centralspindlin pools in which the cortical pool is dominant.

Introduction

Cytokinesis in somatic cells ensures the equal partitioning of the segregated chromosomes and is responsible for the division of the mother cell's cytoplasm into two daughters. This process requires the highly orchestrated assembly and constriction of an acto-myosin contractile ring, usually at the cell's center. The use of various model systems has clearly established that the mitotic spindle defines the position of the contractile ring and the resulting cleavage furrow(von Dassow, 2009, Rappaport, 1971). Two populations of mitotic spindle microtubules (MTs) have been shown to trigger the assembly of the contractile machinery during anaphase. The first is a sub-population of astral MTs. These MTs emanate from the centrosomes to the equatorial cortex where they deliver furrow-inducing signals (Foe and von Dassow, 2008, Vale et al., 2009, Shannon et al., 2005). The second population, comprises the spindle midzone, a region of antiparallel MT overlap and interdigitation within the central spindle that assembles between the decondensing daughter nuclei. In many symmetrically dividing somatic cell types the relative contribution of these two populations has been difficult to unambiguously determine due to their close proximity at the cell's equator. Yet, experiments during the last few decades have led to a proposed common mechanism across model systems in which the furrow-inducing signals emanate from both cortical proximal astral MTs and the spindle midzone with each acting in parallel. However, these pathways do not appear to be equivalent. For instance, if the furrow is initiated at a position distal to the midzone, it will regress and a new one will be established proximal to it (von Dassow, 2009, Foe and von Dassow, 2008, Bringmann and Hyman, 2005, Mishima, 2016). Thus, in equatorially dividing cells, the spindle midzone pathway acts dominantly and can reset furrow position.

Centralspindlin is the main orchestrator of furrowing. This protein complex is a tetramer composed of two subunits of the Kinesin 6 (Pavarotti-klp in *Drosophila melanogaster*) and two subunits of the MgcRacGAP (Tumbleweed in *Drosophila melanogaster*). Tumbleweed is essential for the activation of the Rho-GEF Ect2 (Pebble in *Drosophila melanogaster*). The formation of Rho-GTP triggers the local activation of Rho Kinase and phosphorylation of non-muscle Myosin Regulatory Light Chain, an event that stimulates myosin activation and ultimately drives cytoplasmic cleavage (D'Avino et al., 2015, Glotzer, 2017). While it is well established that centralspindlin acts along central spindle MTs and accumulates at the cell cortex equator to promote symmetrical cleavage, far less is known about how this complex governs asymmetrical divisions. *Drosophila* neural stem cells (Neuroblasts, NBs) are

characterized by a biased furrow placement towards the basal region of the cell. Asymmetric cytokinesis triggers the formation of a large apically positioned cell that retains the NB identity, and a small basal ganglion mother cell (GMC) that will undergo differentiation (Knoblich, 2010). Redistribution of myosin immediately after anaphase onset is the important event that triggers asymmetric cell shape (Cabernard et al., 2010, Connell et al., 2011, Tsankova et al., 2017). Indeed, apical myosin clearing induces apical cortical expansion. This is followed by a basal clearing, which similarly induces an expansion of the basal cortex. This ultimately biases the furrow towards the basal portion of the cell (Cabernard et al., 2010),(Connell et al., 2011). Previous studies have shown that these two processes are under the strict control of the NB polarity machinery and influenced by the spindle midzone and the Chromosome Passenger Complex (CPC) (Roth et al., 2015, Tsankova et al., 2017). To better understand the mechanism of furrow positioning in asymmetrical cytokinesis, we have genetically manipulated spindle size and MT dynamics in *Drosophila* NBs. Our data indicate that the mechanisms dictating asymmetrical daughter cell size are extremely robust and tolerate increases in spindle length and shape. We report that furrowing initiates in a midzone-independent manner, at a basal position through the action of a subcortical centralspindlin pool targeted by peripheral astral microtubules. When these MTs are impaired, centralspindlin recruitment at the furrow is also affected and becomes abnormally enriched at the midzone causing repositioning of the cleavage site, thus affecting the size asymmetry of the daughter cells. Together these results reveal that unlike most systems, in *Drosophila* NBs, which are characterized by a high level of cell size asymmetry during cell division, a population of peripheral astral MTs, and not the spindle midzone, defines and maintains asymmetric cleavage furrow positioning.

Results

Cell size asymmetry is compromised following Ensconsin depletion but not over-expression in NBs

Neuroblasts divide asymmetrically to generate a large self-renewing neuroblast (NB) and a smaller differentiating ganglion mother cell (GMC, Figure 1 A). We previously showed that Ensconsin is required for MT polymerization during cell division; consequently *ensc* mutant spindles are shorter than their wild type (WT) counterparts (Gallaud et al., 2014). To investigate the possible consequences of a change in spindle length on NB asymmetric cell division, we first analyzed, by live cell imaging, cell size asymmetry of dividing NBs in control and *ensc* mutants (Figure 1). We confirmed the previous finding that loss of Ensconsin triggered a ~10% decrease in mitotic spindle length (Figure 1 B, C). Strikingly, the *ensc* mutants displayed a small yet statistically significant reduction in the ratio between NB and GMC diameters indicating a loss of asymmetry (Figure 1 D and J, left). This defect could either result from the associated change in spindle length or indicate some uncharacterized function for Ensconsin in asymmetrical size fate determination. To further explore the role of Ensconsin in MT dynamics *in vitro,* we used TIRF microscopy and recombinant Ensconsin protein (Figure 1 E). Ensconsin-MBP had a small but significant effect on MT growth rate. Most striking was the ~50% reduction in the rate of MT shrinkage and the more than 3 times increase in the rescue frequency compared to controls or MBP alone (Figure 1 F). In line with these results, over-expression of Ensconsin (Ensc-OE) in NBs lead to elongated spindles that buckled when reaching the cortex (Figure 1 G, H, S1), consistent with previous work in symmetrically dividing S2 cells (Gallaud et al., 2014). Despite the increase in MT polymerization and spindle length, the level of size asymmetry remained unperturbed following cytokinesis in Ensc-OE NBs (Figure 1 I, and J, right).

Enhancement of spindle length through over-expression of Msps or depletion of Kinesin-8 MT depolymerase does not alter cell size asymmetry

To determine if daughter cell size asymmetry is insensitive to stimulation of MT growth, we quantified size asymmetry following over-expression of the microtubule associated protein Mini spindles, the fly orthologue of MAP215/ch-TOG, a protein with MT polymerization properties (Reber et al., 2013, Cullen et al., 1999, Fox et al., 2014). In parallel, we performed RNAi-mediated depletion of the MT depolymerizing Kinesin-8 fly family member Klp67A. This kinesin depolymerizes microtubules and its depletion leads to the formation of

exceptionally long spindles in *Drosophila* cells (Goshima et al., 2005, Edzuka and Goshima, 2019). Similar to Ensc-OE, over-expression of Msps-RFP (Msps-OE) or RNAi-mediated depletion of Klp67A led to the formation of long and bent mitotic spindles (Figure 2 A, B and D; Figure S1 A; Video S1 and S2). Neither perturbation affected the post-cleavage asymmetrical cell size (Figure 2 A, C and E). These data suggest that asymmetric cell size regulation is not sensitive to an increase in MT polymer or spindle length elongation.

Spindle shortening through over-expression of Kinesin-8 or -13 MT depolymerases decreases cell size asymmetry

To investigate if the size asymmetry reduction observed in *ensc* mutants (Figure 1) was unique to Ensconsin or rather a common effect of spindle shortening, we induced other perturbations of MT-polymerization by over-expressing two MT depolymerizing kinesins; either Klp10A which belongs to the Kinesin-13 family (Klp10A-OE) or the Kinesin-8 member Klp67A (Klp67A-OE) (Figure S1 A). Importantly, whereas the depletion of either causes spindle elongation, their over-expression results in abnormal shortening (Laycock et al., 2006, Morales-Mulia and Scholey, 2005, Radford et al., 2012, Goshima et al., 2005, Buster et al., 2007). As predicted both Klp10A-OE and Klp67A-OE NBs exhibited shorter spindles although the length reduction was more pronounced in Klp10A-OE cells (Figure 2 F, G, I Video S3). Depending on the spindle's length, it assumed a lesser or greater displacement relative to the cell center. Interestingly, in these shortened spindle cells, like with *ensc* mutants, we found that the NB/GMC diameter ratio was significantly impaired indicating that cell division was more symmetric compared to controls (Figure 2 H and J). Thus, defective MT polymerization leading to spindle shortening due to loss of Ensconsin function or over-expression of the Kinesin- 8s and 13s biases asymmetric cell division. An examination of whole brain phenotypes revealed that ensc mutant brain lobes did not undergo any reduction in NBs. By contrast overexpression of either Klp67A (Figure S1 B) or Klp10A triggered a moderate decrease of NBs (Figure S1 C). This diminished NB number was associated with aneuploidy and polyploidy (Figure S1 D and E). Moreover, we noticed an elevation in cell cycle duration following Klp67A-OE cells (Figure S1 F). Together our data suggest that spindle shortening after Klp10A or Klp67A overexpression compromises cell size asymmetry but also triggers chromosome segregation errors and a loss of NBs.

Defective MT growth leads to an apical shift of the basal cleavage furrow after anaphase onset

In asymmetrically dividing NBs, it was previously demonstrated that polarity- and spindle-dependent pathways ensure appropriate myosin distribution to siblings of different sizes (Cabernard et al., 2010, Roubinet et al., 2017, Tsankova et al., 2017). These two pathways regulate the time between apical and basal myosin clearing and the subsequent apical and basal cortical expansions (Figure S2 A). To investigate the behavior of the furrow, we monitored the dynamics of the regulatory light chain of myosin in live NBs using Sqh-GFP (Royou et al., 2002). In control cells, we confirmed that Myosin-GFP was uniformly present at the cell cortex before anaphase (Figure 3 A and Video S4). In *ensc*, Klp67A-OE and Klp10A-OE NBs, the polarity-dependent apical and basal expansion ratios were similar to controls (Figure S2 B and C). In metaphase NBs with these same genotypes, the cortical polarity appeared unaffected, as judged by the presence of strong aPKC and Miranda crescents at the apical and basal cortices respectively, similar to controls (Figure 2 G). We also examined the polarity-dependent cleavage furrow-positioning pathway, during anaphase transition, which results in apical clearing of myosin. We found that the polarity-dependent apical myosin clearing time was not significantly changed compared to controls (Figure S2 D). We did note a slight dilation in the basal myosin clearing and the time between apical and basal clearing in *ensc* and Klp10A-OE cells (Figure S2 E and S2 F).

We next analyzed furrow positioning through curvature measurements of the cell membrane ((Tsankova et al., 2017) and Figure 3 B). While the furrow position remained stably placed from anaphase until cytokinesis in control NBs, we found it shifted significantly towards the apical side during completion of cell division in *ensc* and Klp67A-OE cells, with a maximal displacement observed for Klp10A-OE NBs (Figure 3, C Video S5 and S6). While the furrow width was consistently ~10% of the half-cell cortex length in control NBs as revealed by Myosin-GFP (Figure 3 D and E), the signal occupied a larger space in *ensc* and Klp67A-OE NBs with the maximum width of ~25% of the half-cell cortex length observed for Klp10A-OE cells at comparable time points (Figure 3 A, E, Video S6). From this we conclude that proper MT growth is required following action of the polarity pathway for maintaining furrow size and position during asymmetrical cell division.

Centralspindlin is spatially and temporally regulated as two distinct populations

Our previous perturbations, which interfered with MT dynamics, suggested that a common mechanism was at play for maintaining the furrow position. In higher eukaryotes, myosin recruitment and activation at the cleavage furrow is regulated by the highly conserved centralspindlin complex, a tetramer comprised of a Kinesin-6 family member complexed with

Mgc-RacGAP (Pavarotti-klp and Tumbleweed in *Drosophila*, respectively)(D'Avino et al., 2015, D'Avino et al., 2005, Mishima, 2016). Strikingly, we found that the combination of Klp10A-OE and a single copy of the pav^{B200} null allele enhanced the asymmetry defect observed with Klp10A-OE alone (Figure S2 H). Centralspindlin functionality and targeting to the membranes is regulated by the chromosomal passenger complex (CPC)-dependent oligomerization (Basant et al., 2015). We therefore challenged the complex by introducing a single null allele for its Survivin subunit, svn^{2180}, and monitored the effects on cell symmetry in the Klp10A-OE background. We found that Klp10A-OE-dependent size asymmetry defects were further enhanced when Survivin levels were reduced (Figure S2 H). These results suggest that the observed asymmetry defects are due, at least in part, to impaired centralspindlin function.

In most eukaryotic cells, the centralspindlin complex is located at the spindle midzone and at the equatorial cortex. To characterize the furrow mis-positioning that accompanies defective microtubule growth, we analyzed the spatiotemporal distribution of the motor component of centralspindlin, Pavarotti-klp, in different experimental backgrounds. We began by examining GFP-Pav-klp (Minestrini et al., 2003) localization in control NBs. Our time-lapse studies showed that most of the GFP-Pav-klp was located at the cortex at the cleavage site (Figure 4 A, E and S3 A). Following the onset of furrow ingression, a second pool started to accumulate into a small and spatially distinct band near the former site occupied by the metaphase chromosomes at the spindle midzone (Figure 4 A, Figure S3A, and Video S7). The spatial and temporal separation of the GFP-Pav-klp signals led us to speculate that these were separate pools of centralspindlin. To confirm this hypothesis, we tracked GFP-Pav-klp in cells lacking MTs that were forced into anaphase using *Mad2* RNAi to abrogate the spindle assembly checkpoint (Gallaud et al., 2014). Under these conditions GFP-Pav-klp showed a slight enrichment at the basal cortex but this pool remained at almost baseline levels compared to control cells, which showed continuous cortical recruitment of GFP-Pav-klp following anaphase onset (Figure S3 B and C). When microtubule polymerization was impaired in *ensc*, Klp10A-OE and Klp67A-OE cells, even if the centralspindlin component GFP-Pav-klp was initially present at the equatorial cell cortex, it did not become enriched at the cleavage site to the levels measured in controls (Figure 4 B, C, E red arrowheads, Figure S4 A, see also Video S8 and S9). Instead, in Klp10A-OE (Video S9), Klp67A-OE but not in *ensc* NBs (Video S8), GFP-Pav-klp was more abundant at the spindle midzone (Figure 4 B and C, see time 100 s blue arrows and insets at time 180 s, Figure 4 E and Figure S4 B). Together, these experiments reveal that centralspindlin exists as two distinct and separable populations, one at

the basal cortex and one at the spindle midzone. The decrease of the cortical centralspindlin pool is always accompanied by a displacement of the cleavage furrow.

The spatiotemporal regulation of centralspindlin relies on stable peripheral MTs

Fluorescence quantification (Figure 4 F) revealed that compared to controls, Klp10-OE and Klp67A-OE NBs both displayed a decrease in cortical GFP-Pav-klp signal with a concomitant increase at the midzone (Figure S4). To further characterize the relationship between cortical and midzone centralspindlin pools and the role of MT growth in asymmetrical cleavage, we examined GFP-Pav-klp dynamics in *sas-4*^{s2214} mutants, which retain an active polarity pathway but lack centrosomes and their associated astral MTs (Cabernard et al., 2010, Basto et al., 2006). In this background, cortical enrichment also appeared diminished relative to the midzone (Figure 4 D, Figure S4 A and B). An enlarged view of the boxed regions for 180 s post-anaphase onset highlights this increased centralspindlin recruitment at the spindle midzone and weaker accumulation at the cell cortex (Figure 4 E). Although *sas-4*^{s2214} NBs exhibited signal enrichment at their midzones, not all cells had a clear cortical reduction (Figure S4). In addition, *sas-4*^{s2214} mutants exhibited both an increased spindle length as well as a significant overall cell size asymmetry defect (Figure S5 A and B), further supporting the idea that MT-asters maintain basal furrow position. Similar to previous studies, the cortico-basal expansion ratios were unchanged in *sas-4*^{s2214} NBs (Connell et al., 2011). This indicates that the centrosome associated MT asters are also important for furrow positioning (Figure S5 D). To confirm the contribution of MT-asters in furrow positioning and maintenance, we removed them through laser ablation of the apical and basal centrosomes. Each centrosome was labeled with GFP-tagged Aurora A and apical and basal centrosomes were irradiated by a multi-photon laser until the signal was no longer detectable. Sample fixation and immunostaining post-ablation showed the complete disappearance of the Cnn-labeled centrosome and its associated astral microtubule aster (Figure S5 E, arrowhead). Consistent with centrosome removal, ablated cells displayed a phenotype virtually identical to *sas-4*^{s2214} mutants: daughter cells exhibited cell size asymmetry after the ensuing cytokinesis (Figure S5 F, G, Video S10, compare left and right). These live cell observations suggested that astral MTs were essential to cleavage furrow positioning. Accurate quantification of MTs in live cells was precluded by the lack of spatial resolution in our recordings. We therefore performed a quantitative analysis of fixed preparations. Although fixed cell approaches can introduce unintentional bias due to different substage durations that can mask subtle MT dynamic changes, large-scale trends and differences will be preserved. Detailed morphological

examination revealed that in control NBs, bundles of astral MTs were closely apposed to the cortex at the cleavage furrow. This was not the case with *ensc*, Klp67A-OE or Klp10-OE NBs, all of which showed decreased MT densities and lacked the presumptive bundles (Figure S5 H and I). Taken together our data strongly suggest that peripheral astral MTs originating from the apical and basal centrosomes play a key role in inducing asymmetric cell division.

Depletion of the spindle midzone protein Feo does not trigger furrow-positioning defects

The presence of GFP-Pav-klp at the spindle midzone distal to the cleavage site and the movement of the furrow towards the equator in peripheral MTs-deficient cells prompted us to further characterize the cleavage site and the midzone in control cells. For this purpose, we used Fascetto-GFP (the homologue of the mammalian PRC1 protein; Feo-GFP) a marker that uniquely labels the spindle midzone (Figure 5 A) (Verni et al., 2004, Wang et al., 2015). We found that in these NBs the metaphase plate was slightly shifted toward the basal side relative to the cell equator along the apico-basal axis (Figure 5 A, -120 s, blue arrowhead and Figure 5 C, left) but similarly placed to the midzone-defining Feo-GFP signal that appears following anaphase chromosome segregation (Figure 5 A, time 60 s, Figure 5B and Figure 5 C middle). This was in contrast to the position of the cleavage furrow (Figure 5 A, time 90, compare green and red arrowheads; Figure 5 B, 5 C, right), which was always distinct and basally distal to the midzone (Figure 5 D, Video S11). Kymograph analyses of the spindle midzone and cell membranes revealed that the midzone moves basally during the ingression of the furrow until they ultimately consolidate into a single structure (Figure 5 B). These distribution data raise the possibility that Feo and the spindle midzone may not contribute to furrow positioning in wild type NBs. We therefore assayed if Feo depletion and spindle midzone destabilization could impair furrow positioning and asymmetric cell division. We found that Feo-depleted NBs (Figure 5 E) did not exhibit furrow-positioning defects during anaphase (Figure 5 F and G) and the final NB/GMC diameter ratio was similar to controls (Figure 5 H). However, 22% (4/18) of Feo-depleted NBs exhibited late cytokinesis failure (Figure S6 A). Thus spindle midzone MTs appear to play a key role during the late steps of cytokinesis rather than in furrow positioning during anaphase. In parallel, we analyzed if the midzone was reinforced following astral MT depletion (Figure 5 I and J, Figure S6 B). The Feo-GFP signal intensity at the midzone was enhanced in Klp10A-OE NBs (Figure 5I and S6 C) but remained unchanged in Klp67-OE and *sas-4*^{s2214} NBs. In addition, the signal was decreased in *ensc* mutant NBs (Figure S6 C). Moreover, the spindle midzone signal was significantly longer in

303 *ensc*, Klp10A-OE, Klp67-OE and *sas-4*^{s2214} NBs (Figure S6 D). Interestingly, we also
304 observed that mitotic spindle length was restored after metaphase and was similar to telophase
305 controls in Klp10A-OE NBs (Figure S6 E). In these NBs furrow displacement toward the
306 apical cortex was accompanied by a reduced midzone movement toward the basal cortex
307 (Figure S6 F). In summary, these data demonstrate that the spindle midzone in NBs occupies
308 a spatially different position than that of the furrow and its associated cortical MTs. Both of
309 these MT structures can recruit centralspindlin, however, under normal circumstances in
310 *Drosophila* NBs it is the cortical pool that dominates to define the cleavage site (Figure S6
311 G).

Discussion

Asymmetric cell division is a robust process that ensures that two daughter cells inherit different fates and sizes. The *Drosophila* NB is a powerful and widely used model system to study this specialized form of division because of the large number of NBs in the developing *Drosophila* brain, rapid division time and experimental tractability (Rusan and Peifer, 2007, Januschke and Gonzalez, 2008, Rebollo et al., 2007). Although these cells are relatively small, they are highly asymmetrical following cytokinesis allowing accurate measurements and analyses. In this study, we have challenged asymmetric cell division in this model system by modifying MT growth dynamics. We were able to increase mitotic spindle length using over-expression of MT polymerizing MAPs (Msps and Ensconsin), as well as by RNAi-mediated depletion of Klp67A, a member of the Kinesin-8 family of MT depolymerizing Kinesins. Despite the presence of long and bent mitotic spindles under these conditions, the NB cell size ratio remained unchanged relative to control NBs. This reveals that asymmetric cell division and asymmetric positioning of the cleavage furrow are resistant to an excess of abnormally long and stable MTs during cell division. By contrast, decreasing MT stability and shortening the mitotic spindle produced more symmetric cell divisions. This change was due to an apical shift of the cleavage furrow during its ingression, following apical and basal cortex expansion. This phenotype was not MAP-dependent and was observed following over-expression of either Klp10A (Kinesin-13) or Klp67A (Kinesin-8) MT depolymerases and in *ensc* mutants. Rather the data suggest that spindle size or interference with microtubule dynamics is responsible for the phenotype. In agreement with this spindle size is restored in Klp10A-OE telophase cells, which display the shortest spindles at metaphase (Figure S6 E). Interestingly, *sas-4*^{s2214} mutants which are reported to lack functional centrosomes and thus astral microtubules yielded reduced levels of cell size asymmetry despite harboring longer metaphase spindles (Basto et al., 2006). This suggests that MT asters and not spindle length are the key determinant factor for size asymmetry in NBs. Consistent with this, loss of either apical and basal MT-aster, through targeted laser irradiation and ablation prior anaphase onset, also reduced sibling cell size asymmetry. Together these results strongly suggest that astral MTs are required to maintain a cleavage site, which normally favors a basal position in the fly neuroblast. We propose that a specific population of these astral microtubules, called peripheral microtubules, are positioned in direct contact with the division furrow and plays a determining role in maintaining its stable position during anaphase till cytokinesis. For technical reasons, we were unable to quantify peripheral MTs bundles in live dividing cells.

However, fixed cell quantitative, despite a possible bias in the determination of late anaphase sub stages, support this and revealed a significant decrease in peripheral MTs during in *ensc*, Klp10A-OE and Klp67A-OE NBs (Figure S5). Our results are in accord with reports indicating that a subpopulation of these stable astral MTs play a key role in the initiation of furrowing in symmetrically dividing cells and that in some systems, furrowing can occur without the presence of a stable central spindle (Murthy and Wadsworth, 2008, Foe and von Dassow, 2008, Strickland et al., 2005, Canman et al., 2003, Inoue et al., 2004, Bringmann and Hyman, 2005, Kotynkova et al., 2016, Mishima, 2016). However, in contrast to previous studies, our data reveals that in asymmetrically dividing control NBs, the astral MT furrowing pathway dominates over the midzone pathway. Prior investigations indicated that NBs have two genetically separable pathways to drive cytokinesis. The first, the polarity-dependent pathway triggers the clearing of apical myosin, resulting in apical cortical expansion. Interference with this pathway leads to simultaneous apical and basal clearing, symmetrical cortex expansion, equatorial furrow positioning and to a symmetric division (Cabernard et al., 2010, Roth et al., 2015, Connell et al., 2011). The second, spindle pathway, is proposed to rely on the spindle midzone and the chromosomal passenger complex. This triggers the subsequent basal myosin clearing and basal cortical expansion ((Roth et al., 2015) and Figure S2 A). Several of the results presented here lead us to propose another additional mechanism for furrow positioning that would rely on peripheral astral MTs with a minor contribution from the spindle midzone. This is supported by several of our observations: (i) live cell imaging and analyses utilizing GFP-Pav-klp as a marker of centralspindlin position revealed that this master controller of cytokinesis accumulated at the basal cortex throughout the entire furrow ingression process (this paper and (Cabernard et al., 2010)). (ii) Centralspindlin levels were low at the midzone during furrow placement and ingression compared to the cortex (Figure 4). (iii) We consistently found that the midzone, as defined independently using both GFP-Pav-klp and Feo-GFP, was spatially independent from the furrowing site (Figures 5 B, 6 A). Moreover, inhibition of midzone formation through Feo depletion did not impair furrow positioning but did interfere with the late stages of cytokinesis. (iv) The midzone consistently relocated from an initial location to a final position that was coincident with the furrow. The converse was never observed (Figure 5 B), confirming previous observations made in embryonic NBs (Kaltschmidt et al., 2000). (v) Finally, genetic or photo-based interference with centrosomes precluded astral MT formation and interaction with the cortex. Accordingly, the cortical centralspindlin pool was diminished and NBs exhibited a size asymmetry defect (Figure 4 and S4).

Our localization studies suggest that under normal conditions midzone-associated centralspindlin does not perform a key role in positioning of the cleavage site and that this function is served by the more abundant centralspindlin pool associated with the cortex at the cleavage site. When astral MTs were impaired, centralspindlin enrichment at the furrow was often diminished, and in some cases accompanied by an increase in the midzone-associated pool, leading to a decreased midzone/furrow centralspindlin ratio and a reset of the furrowing toward the equatorial midzone. This indicates that the two populations of centralspindlin are competent to signal furrowing but that the cortical pool delivered by astral MTs may be dominant. Thus the spatial localization and the cortical/midzone ratio of centralspindlin are the pivotal determinants of final furrow position in the *Drosophila* NB. Interestingly, a recent study has shown that a similar competition between centralspindlin pools also occurs in human cells, revealing an evolutionary conservation of the mechanism (Adriaans et al., 2019). As with human cells, we found that the CPC activity seems essential in this regulatory event (Figure S2 C).

In contrast to a recent study in the symmetrically dividing S2 cells, we do not observe GFP-Pav-klp labeling at the plus ends of astral MTs (Vale et al., 2009, Verma and Maresca, 2019) even when studied by enhanced resolution imaging methods. Instead, we consistently find that centralspindlin coats the entire length of astral MTs emanating from both centrosomes, suggesting that the plus end directed motor activity of Pav-klp is used to bring centralspindlin to the furrow in *Drosophil*a NBs similar to findings in early embryos (Minestrini et al., 2003, Minestrini et al., 2002). It is therefore likely that centralspindlin, depending on the cell type utilizes preferentially EB1-mediated MT plus ends or the motor activity of Pav-Klp to reach the cleavage site.

In total our data suggest a model in which competition between different centralspindlin populations is a key determinant of asymmetric division in *Drosophila* NBs. The consecutive action of the polarity-dependent cleavage furrow-positioning pathway and the MTs emanating from the asters serving as centralspindlin delivery arrays are essential in the whole process. In this system, we propose that the ability of the spindle midzone to define furrow and cleavage location may only become engaged during late telophase or after subcortical astral MTs are compromised. Despite their clear role in governing size asymmetry, we have not been able to induce complete daughter cell size equality through any of a host of MT perturbing treatments. It is possible that the few MTs that remain after our perturbations are sufficient to target enough cortical centralspindlin to provide some degree of asymmetry. However, additional mechanisms, such as MT initial asymmetric midzone position and displacement

toward the cleavage site also appears important to secure a minimal level of asymmetry in these cells (Figure S6 F). Elucidating these systems and their advantages for asymmetrically dividing stem cells will be important directions for future investigations on tissue homeostasis.

Limitation of this study

Our study reveals a critical role for astral MTs in maintaining the asymmetric position of the cleavage site during cytokinesis in neural stem cells. This is essential to preserve an appropriate Neuroblast/GMC cell size ratio. We find that the perturbation of astral MTs and the subsequent loss of asymmetry occur in the presence of a timely apical myosin clearing, an event regulated by the polarity-dependent pathway that controls apical cortical expansion during anaphase. However, we cannot fully rule out that our observations are completely polarity independent. Other additional yet uncharacterized polarity-dependent mechanisms could be involved to contribute to our findings. Indeed, it remains possible that polarity proteins participate in the regulation of other components including centrosomal or MT-associated proteins, to control the dynamics of these peripheral astral MTs and ultimately basal furrow positioning.

Acknowledgments

We thank Gregory Rogers, Pier Paolo d'Avino, Renata Basto, Gohta Goshima, Jordan Raff, Hiro Ohkura, Anne Royou, Roger Karess, Christian Dahmann, Antoine Guichet, Juliette Mathieu, Jean-René Huynh, Clemens Cabernard, Tri Pham for providing fly stocks, antibodies, cDNAs and useful advices. We thank Chloé Rauzier for preliminary functional analyzes of Ensc-OE and Msps-OE NBs. This work was funded by the Ligue Nationale Contre le Cancer, the Fondation ARC pour la Recherche sur le Cancer. A. T. is a doctoral fellow of the Région Bretagne and the Ligue Nationale contre le Cancer. We thank the Photonic Imaging Center of Grenoble Institute of Neurosciences, which is part of ISdV core facility. We thank Xavier Pinson, Stéphanie Dutertre and Sébastien Huet for advices and help with the microscopes and the Microscopy Rennes Imaging Center platform. We thank Romain Gibeaux, Pier Paolo d'Avino and Christelle Benaud for ideas, critical readings and helpful suggestions. The authors have no competing financial interests to declare.

Author contributions

Conceptualisation, A.T., R.G; Methodology, A.T., E.G., I.A., R.G. Investigation, A.T., A.P., E.G., L.S., I.A., R.G.; Writing, A.T and R.G; Review & Editing, A.T., E.G., M.S.S., R.G; Funding Acquisition, R.G; Resources, R.G; Supervision, L.R-P., R.G.

Declaration of interest

The authors have no interest to declare.

Main figure titles and legends

Figure 1. Analysis of cell size asymmetry in *ensc* and Ensc-OE NBs

A) Scheme of a NB during cell division during metaphase (left) and telophase (right). Note that the NB cell division is asymmetric and produces a large NB and a small Ganglion Mother Cell (GMC) during cytokinesis. B) Selected images of a control NB (top) and an *ensc* mutant NB (bottom) during cell division. The membranes are displayed in green and the MTs are displayed in magenta. Time is min:s. Scale bar: 10µm. C) Dot plot showing the mean (± s.d.) mitotic spindle length/NB diameter ratio in control (0.86±0.05, n=27) or in *ensc* NBs (0.79±0.06, n=23), ***: P<0.0001 (Mann-Whitney test). D) Dot plot showing the NB mean (± s.d.) diameter/GMC diameter ratio in control (2.29±0.20, n=27) or in *ensc* NBs (2.16±0.20, n=23), *: P<0.05 (Mann-Whitney test). E) Kymographs showing microtubules assembled from GMPCPP seeds and 14 µM tubulin in absence or in presence of 200 nM of MBP or MBP-Ensconsin. Horizontal and vertical scale bar are 5µm and 60s respectively. F) Graphs showing the mean (± s.d.) growth and shrinkage rates and the catastrophe and rescue frequencies determined from kymographs shown in E. ns: non significant; ****: P<0.0001 (Kruskal-Wallis ANOVA followed by post-hoc Dunn's multiple comparison, total number of growth events = 116, 123 and 107, shrinkage events = 67, 73 and 81, catastrophe events = 94, 96, 83 and rescue events = 3, 3 and 33 for the control, MPB and MPB-ensconsin respectively). G) Selected images of a control NB (top) and an Ensc-OE NB (bottom) during cell division. Membranes are displayed in magenta and MTs or Ensconsin are displayed in green. H) Dot plot showing mean (± s.d.) the mitotic spindle length/NB diameter ratio in control (0.86±0.06, n=25) or in Ensc-OE NBs (0.95±0.08, n=19), ****: P<0.0001 (Mann-Whitney test). I) Dot plot showing the mean (± s.d.) NB diameter/GMC diameter ratio in control (2.36±0.17, n=25) or in Ensc-OE NBs (2.40±0.19, n=19), ns: non-significant (Mann-Whitney test) J) Summary of NB division in *ensc* (left) or Ensc-OE (right). *ensc* mutant NBs display shorter spindles and undergo less asymmetric cell division while Ensc-OE NBs, despite harboring long spindles, divides asymmetrically similar to WT. Time is min:s. See also Figure S1.

Figure 2. Analysis of cell size asymmetry in NB following modification of several MAP protein levels

A) Selected images of control (top), Msps-OE (middle) and *Klp67A* RNAi (bottom) NBs. The membranes are shown in green, the MTs (top and bottom) and Msps (middle) are shown in

magenta. Time is min:s. Scale bar: 10µm. B) Dot plot showing the mitotic spindle length/NB diameter ratio (± s.d.) in the NB of control (0.86±0.06, *n*=18) or in Msps-OE transgenic flies (1.03±0.1, *n*=23), ****: *P*<0.0001 (Mann-Whitney test). C) Dot plot showing the mean (± s.d.) NB diameter/GMC diameter ratio in control (2.34±0.16, *n*=18) or in Msps-OE NBs (2.29±0.28, *n*=21), ns: non-significant (Mann-Whitney test). D) Dot plot showing the mean (± s.d.) mitotic spindle length/NB diameter ratio in control NBs (0.83±0.07, *n*=40) or in *Klp67A* RNAi NBs (1.19±0.15, *n*=30), ****: *P*<0.0001 (Mann-Whitney test). E) Dot plot showing the mean (± s.d.) NB diameter/GMC diameter ratio in control (2.31±0.16, *n*=40) or in *Klp67A* RNAi NBs (2.32±0.23, *n*=30), ns: non-significant (Mann-Whitney test). F) Selected images of control (top), Klp10A-OE (middle) and Klp67A-OE (bottom) NBs. The membranes are shown in green, the MTs are shown in magenta. Scale bar: 10µm. Time is min:s. G) Dot plot showing the mean (± s.d.) mitotic spindle length/NB diameter ratio in control NBs (0.79±0.08, *n*=49) or in Klp10A-OE NBs (0.63±0.09, *n*=49), ****: *P*<0.0001 (Mann-Whitney test). H) Dot plot showing the NB diameter/GMC diameter ratio (± s.d.) in control NBs (2.29±0.17, *n*=49) or in Klp10A-OE NBs (2.00±0.27, *n*=49), ****: *P*<0.0001 (Mann-Whitney test). I) Dot plot showing mean (± s.d.) the mitotic spindle length/NB diameter in control NBs (0.83±0.07, *n*=40) or in Klp67A-OE NBs (0.73±0.08, *n*=48), ****: *P*<0.0001 (Mann-Whitney test). J) Dot plot showing the mean (± s.d.) NB diameter/GMC diameter ratio in control NBs (2.32±0.16, *n*=40) or in *Klp67A* RNAi NBs (2.19±0.18, *n*=48), ***: *P*<0.0001 (Mann-Whitney test). See also Figure S1.

Figure 3. Analysis of myosin dynamics and furrow positioning in *ensc*, Klp67-OE and Klp10A-OE

A) Selected images of (from top to bottom) dividing control, *ensc*, Klp67A-OE and Klp10A-OE NBs expressing tubulin (magenta) and myosin regulatory light chain (green and lower panels in monochrome) after anaphase onset (t=20s) till late telophase. Scale bar: 10µm. Time is s. B) Scheme showing the possible apical shift between the initial and final furrow curvature analysis. C) Dot plot showing mean (± s.d.) of the relative furrow displacement between early anaphase and late telophase in control (0.00±0.04, *n*=18), *ensc* (-0.03±0.05, *n*=18), Klp67A-OE (-0.05±0.04, *n*=12), and Klp10A-OE NBs (-0.14±0.04, *n*=22). *: *P*<0.05, ***: *P*<0.001, ****: *P*<0.0001 (Mann-Whitney test). D) Scheme showing the furrow width (red) during mid anaphase. E) Dot plot showing the mean (± s.d.) relative myosin furrow width/cell length ratio for control (0.08±0.02, *n*=18), *ensc* (0.14±0.07, *n*=17), Klp67A-OE

(0.13±0.05, n=12), and Klp10A-OE NBs (0.25±0.11, *n*=23), *: *P*<0.05, ***: *P*<0.001, ****: *P*<0.0001 (Mann-Whitney test). See also Figure S2.

Figure 4. Analysis of centralspindlin localization and dynamics in control, *ensc*, Klp10A-OE and *sas-4^{s2214}* NBs

A) Selected images of dividing control expressing tubulin (magenta) and GFP-Pav-klp (green and lower panels in monochrome) from anaphase onset till late telophase (top left). B) *ensc* NB. C) Klp10A-OE NB. D) *sas-4^{s2214}* NBs (bottom). Scale bar: 10µm. Time is s. E) Higher magnification view of the selected control *ensc*, Klp10A-OE and *sas-4^{s2214}* telophase NBs (from panels in A-D) showing GFP-Pav-klp localization at the cleavage site. See the strong signal at the cell cortex (red arrowheads) and the weak signal at the presumptive spindle midzone away from the cleavage site, toward the apical side blue (blue arrows). F) Scheme of the cleavage site showing the cortical and midzone centralspindlin pools. G) Dot plot showing the mean (± s.d.) relative cortical/midzone GFP intensity ratio for control (2.21±0.89, *n*=15), *ensc* (1.57±0.70, *n*=11), Klp10A-OE (1.09±0.61, *n*=10), *sas-4^{s2214}* (0.84±0.35, *n*=10), control (3.24±1.40, *n*=7) and Klp67A-OE NBs (1.77±0.55, *n*=11). *: *P*<0.05, ***: *P*<0.001, ****: *P*<0.0001 (Mann-Whitney test). See also Figures S3, S4 and S5.

Figure 5. Analysis of the spindle midzone and the cleavage furrow position in brain NBs during cell division

A) Selected images of a WT NB expressing Feo-GFP (green and lower panels in monochrome), MTs (magenta), and membranes during cell division (green and lower panels in monochrome). The metaphase plate is indicated by a blue arrowhead (-120s). Red arrowheads indicate the spindle midzone and the furrow is indicated by green arrowheads (60-300s). Scale bar: 10 µm. Time is s. B) Kymograph showing the localization of the spindle midzone and the cell contours during the time course of the NB cell division shown in panel A, along the apico-basal axis. Vertical scale bar: 5 µm. C) Dot plot showing the mean (± s.d.) relative metaphase plate position along the apico-basal cortex 90 s after anaphase onset (left: 0.56±0.02 *n*=21) the mean (± s.d.) relative spindle midzone position along the apico-basal cortex 90 s after anaphase onset (middle: 0.59±0.02, *n*=23) and the mean (± s.d.) relative furrow position along the apico-basal cortex 90 s after anaphase onset (right: 0.72±0.13, *n*=23). D) Dot Plot showing the mean (± s.d.) relative distance between the furrow and the spindle midzone 90 s after anaphase onset (0.13 ± 0.02, *n*=23). E) Western blot of Feo (top) and actin (bottom) protein levels in control or *Feo* RNAi brains. F) Control (top) or *Feo*

RNAi NBs expressing PH-PLCδ-GFP (green and bottom panels in monochrome) and mCherry-tubulin (magenta). G) Dot plot showing the mean (± s.d.) relative midzone position for control (0.69±0.03, *n*=16) and *Feo* RNAi NBs (0.69±0.02, *n*=18). Ns: not significant unpaired T test. H) Dot plot showing the mean (± s.d.) NB/GMC size ratio for control (2.36±0.12, *n*=16) and *Feo* RNAi NBs (2.40±0.15, *n*=14). Note late cytokinesis failed in 4/18 NBs (22%). Ns: not significant (Unpaired T test). I) Selected frames of a control (top) or a Klp10A-OE NB expressing Feo-GFP (green and bottom panels in monochrome) and mCherry-tubulin (magenta) after anaphase onset (0 s). Arrowheads indicate midzone-associated Feo-GFP. Scale bar: 10 μm. Time is s. J) Dot plot showing the mean (± s.d.) time (s) between Feo-GFP detection on the midzone and basal myosin clearing in control (59.4±15.4, *n*=18) and Klp10A-OE (108.7±40.5, *n*=15) Nbs. ****: P<0.0001 (Mann-Whitney test). See also Figure S6.

STAR Methods

RESOURCE AVAILABILITY

Lead Contact

Further information and requests for reagents generated in this study should be directed to and will be fulfilled by the Lead Contact, Régis Giet (regis.giet@univ-rennes1.fr).

Materials Availability

All unique/stable reagents generated in this study are available from the lead contact without restriction.

Data and Code Availability

§ All data reported in this paper will be shared by the lead contact upon request.

§ This paper study does not report original code.

§ Any additional information required to reanalyze the data reported in this work paper is available from the Lead Contact upon request.

EXPERIMENTAL MODELS AND SUBJECT DETAILS

Fly strains

All flies were maintained under standard conditions at 25°C. The *ensconsin* mutant fly stocks *enscΔnull* and *enscΔN*, referred to *ensc* flies, were characterized previously (Gallaud et al., 2014). UAS-Ensconsin-Venus transgenic flies have been characterized in a previous study (Metivier et al., 2019). UAS-Msps-RFP overexpressing flies were obtained from BestGene (USA) following P-element mediated transformation. UAS-Klp10A flies were supplied by C. Dahmann (Max Planck Institute, Germany) (Widmann and Dahmann, 2009). UAS-Klp67A (ID # F001232) stock was obtained from FlyORF (Bischof et al., 2013). UAS-Klp67A-RNAi (VDRC ID 52105) and UAS-Mad2-RNAi (VDRC ID 106003) transgenic fly lines were obtained from the Vienna Drosophila RNAi Center (Dietzl et al., 2007). Sqh-GFP (Royou et al., 2002), UAS-GFP-Pav-klp (Minestrini et al., 2003) and Ubiquitin-β-tub-GFP expressing flies (Inoue et al., 2004, Minestrini et al., 2003) were supplied by R. Karess (Institut Jacques Monod, France) and by D. Glover (University of Cambridge, UK), respectively. The Pavarotti mutant pav^{B200} flies were obtained from E. Montembault (Institut Européen de Chimie et Biologie, France) (Adams et al., 1998) and the Survivin mutant allele svn^{2180} flies were courtesy of Jean-René Hyunh (College de France, France) (Mathieu et al., 2013). Flies expressing the membrane-localized PH-PLCδ-GFP and PH-PLCδ-RFP proteins were provided by A. Guichet (Institut Jacques Monod, France) (Claret et al., 2014, Gervais et al.,

2008). RFP-Tubulin flies were provided by R. Basto (Institut Currie, France). The GFP-AurA expressing fly stock was described previously (Caous et al., 2015). The following stocks were obtained from the Bloomington Stock Center: Feo-GFP expressed under the ubiquitin promoter (BDSC 59273, (Wang et al., 2015)), *sas-4*^{s2214} mutant (BDSC 12119, (Basto et al., 2006)), 69B-Gal4 (BDSC 1774), Insc-Gal4 (BDSC 8751), UAS-mCherry-α-tubulin (BDSC 25774 and BDSC 25773). The *Feo* RNAi stock was from the Vienna Drosophila RNAi Center (VDRC 107824). The 69B-Gal4 fly stock was used to drive over-expression in the fly CNS for the following UAS regulated transgenes: Klp67A, Msps, GFP-Pav-Klp together with *Mad2* RNAi and UAS-mCherry at 25°C for 3 days and 2 days at 29°C for *Feo* RNAi. The Insc-Gal4 strain was used to drive over-expression of Ensconsin, Klp10A, UAS-GFP-Pav-klp and mCherry-α–tubulin transgenes in the central brain at 25°C.

METHOD DETAILS

Molecular biology

Msps cDNA was provided by G. Rogers (University of Arizona, USA), amplified by PCR and inserted into pDONR221 (Life Technologies) to generate the pDONR221-Msps entry clone. pENTR-Ensc has been previously described (Gallaud et al., 2014). pDONR221-Msps entry clone was subsequently recombined into pTWR (Carnegie Institute, USA) using the Gateway recombination cloning technology (Life Technologies) to generate a construct allowing the expression of Msps-RFP fusion proteins under the control of the GAL4 protein. pENTR-Ensc was recombined into pDEST-MBP (a gift from H. Ohkura, University of Edinburgh, UK) to allow the expression of a recombinant Ensconsin protein with a C-terminal Maltose Binding Protein tag.

Production of recombinant proteins

MBP and Ensconsin-MBP were induced in *E. coli*, for 4 h at 25°C. The proteins were purified on amylose columns as described by the manufacturer (BioLabs) and stored in small aliquots at -80°C.

TIRF microscopy and analysis of MT dynamics

Tubulin was purified from bovine brain and fluorescently labeled with ATTO 488 and ATTO 565 or biotinylated as described before (Hyman et al., 1991, Ramirez-Rios et al., 2017).

637 Briefly, microtubule seeds were prepared from biotinylated and ATTO-565-labeled tubulin in
638 the presence of Guanosine-5'-[(α,β)-methyleno]triphosphate (GMPCPP) in BRB80 buffer (80
639 mM Pipes, 1 mM EGTA, 1 mM $MgCl_2$, pH 6.74) (Ramirez-Rios et al., 2017). Flow chambers
640 were prepared with functionalized silane-PEG-biotin coverslips and silane-PEG glass slides,
641 as previously described (Ramirez-Rios et al., 2017). The chamber was successively perfused
642 at room temperature with neutravidin (25 µg/ml in 1% BSA in BRB80), PLL-g-PEG (2 kD,
643 0.1 mg/ml in 10 mM Hepes, pH 7.4), BSA (1% in BRB80 buffer) and microtubule seeds. The
644 following assembly mixture was then injected: 14 µM tubulin (containing 15 % ATTO-488-
645 labeled tubulin) without or with 200 nM MBP or MBP-Ensconsin in TIRF assay buffer (4 nM
646 DTT, 50 mM KCl, 1% BSA, 1 mg/mL glucose, 70 µg/mL catalase, 580 µg/mL glucose
647 oxidase, 0.05% methylcellulose (4000 centipoise) in BRB80). Time-lapse images were
648 recorded at 35°C at a rate of one frame per 5 seconds on an inverted Eclipse Ti Nikon
649 microscope equipped with an Apochromat 60X1.49 N.A oil immersion objective, an iLas^2
650 TIRF system (Roper Scientific), and a cooled charge-coupled device camera (EMCCD
651 Evolve 512, Photometrics) controlled by MetaMorph 7.7.5 software.
652 Microtubule dynamic parameters were analyzed in Image J on kymographs obtained using an
653 in-house KymoTool macro (available upon request to eric.denarier@univ-grenoble-alpes.fr).
654 Growth and shrinkage rates were determined from the slopes of microtubule growth and
655 shrinkage phases. The catastrophe and rescue frequencies were calculated by dividing the
656 number of events per microtubule by the time spent in growing and shrinking states,
657 respectively.
658
659 **Antibodies and Western blotting**
660 The following antibodies and concentrations were used in this study: polyclonal rabbit anti-
661 Msps (1:5000) provided by J. Raff (Lee et al., 2001), polyclonal rabbit anti-Klp67A (1:500)
662 supplied by G. Goshima (Goshima and Vale, 2005), polyclonal rabbit anti-Feo antibody
663 (1:2000) was provided by J. Scholey (Wang et al., 2015), polyclonal rabbit anti-Klp10A
664 (1:1000) was courtesy of G. Rogers (Mennella et al., 2005) and rabbit anti-Myosin (1:2000)
665 was provided by R. Karess (Jordan and Karess, 1997). The anti-Ensconsin antibody raised
666 against the Kinesin binding domain has been previously described(Gallaud et al., 2014).
667 Rabbit anti-PKCζ (C-20, 1:200) and anti-actin polyclonal antibodies (sc-1616, 1:5000) were
668 obtained from Santa Cruz Technology. Monoclonal mouse anti-alpha Tubulin (clone DM1A,
669 T2199; 1:500) and rabbit polyclonal anti-phosphorylated histone H3 (Ser10) (06570, 1:500)
670 antibodies were obtained from Millipore. Monoclonal rat anti-Miranda antibody (ab197788,

1:1000) was obtained from Abcam. Rat anti-Deapan (AB195173, 1:100) and mouse anti-Propero (MR1A, 1:500) antibodies were from DSHB. Secondary antibodies were labeled with either Alexa Fluor-conjugated (1:1000) or peroxidase-conjugated secondary antibodies (1:5000), each obtained from Life Technologies. For Western Blotting ECL reagents were purchased from ThermoFisher.

Live cell microscopy

Third-instar larval brains were dissected in Schneider's Drosophila medium supplemented with 10% FCS. Isolated brains were loaded and mounted on stainless steel slides, and the preparations were sealed with mineral oil (Sigma-Aldrich) as previously described (Gallaud et al., 2014). For MT depolymerization experiments, larval brains were incubated during 30 min in the above medium supplemented with colchicine at a final concentration of 15 µM. After incubation, brains were mounted and processed for live cell imaging.

Images were acquired at 25°C using a CSU-X1 spinning-disk system mounted on an inverted microscope (Elipse Ti; Nikon) equipped with a 60X 1.4 NA objective. At 20, 30 or 60 s intervals 10 z-steps were acquired with 1µm intervals. Fluorescent protein probes were excited with 488nm or 561nm laser light and the images were captured using a sCMOS ORCA-Flash4.0 (Hamamatsu) camera. Recordings were controlled using MetaMorph acquisition software. Alternatively, images were acquired with a spinning disk system consisting of a DMi8 microscope (Leica) equipped with a 63X (1.4 N.A.) oil objective, a CSU-X1 spinning disk unit (Yokogawa) and an Evolve EMCCD camera (Photometrics). The microscope was controlled by the Inscoper Imaging Suite and the dedicated software (Inscoper). Data were processed in ImageJ and viewed as maximum-intensity projections prior to analysis or figure preparation.

Photo-ablation experiments

Photo-ablations were performed with a Mai-Tai two-photon infrared laser (Spectra Physics) attached to a Leica SP5 confocal microscope equipped with a 60X 1.3 NA objective with the stage maintained at 25°C. *Z*-series consisting of 10, 1µm steps were acquired before and after the photo-ablation at 30 s intervals. Photo-ablation was performed on the basal and apical centrosomes using flies expressing GFP-H2A, PH-PLCδ-GFP and Aurora A-GFP. Anaphase onset was identified as the first signs of sister chromatid separation. The rapid (<10 s, (Berdnik and Knoblich, 2002)) recovery of Aurora A-GFP was used to differentiate between centrosome photo bleaching and photo-ablation. Photo-ablation efficacy was confirmed using

cells co-expressing RFP-tubulin. Cells that did not recovery the Aurora A-GFP signal within 30 s post-irradiation also displayed a loss of the MT-aster as reveled in live and fixed cell analyses.

Live cell imaging analysis

Measurements of fluorescence intensities, distances, mitotic spindle lengths and diameters of NB and GMC cells were performed with ImageJ software (Rueden et al., 2017). The Sqh-GFP analyses were done on the maximum projection of two optical sections (1 µm). The cortical GFP-Pav-klp intensity analyses on the furrow during anaphase were calculated as the mean normalized intensity signal between the two sides of the furrow on two optical sections (1 µm). Cell cycle duration was calculated as the time between two consecutive NEBD events. The polarity-dependent apical and basal clearings were calculated, as the time point after anaphase onset, when myosin disappeared from the apical and basal cortices respectively (Connell et al., 2011),(Roubinet et al., 2017). NB cortex curvature analyses were performed according to previously defined methods (Tsankova et al., 2017). The furrow shift was determined as the distance between the first ingression site and final cleavage site. To quantify the Myosin-GFP furrows width; a segmented line was drawn along the NB half-cell cortex during anaphase and the GFP intensity profiles were quantified along this line using ImageJ. The furrow width was measured as the relative half-cell cortex length containing 60% of the maximum Sqh-GFP signal intensity. Cortical expansion analyses were performed as described previously (Connell et al., 2011). Detailed analyses are illustrated in Figure S2A.

Immunofluorescence analysis

Larval brains from each genotype were processed for immunofluorescence studies as described previously (Gallaud et al., 2014). Briefly, wandering third instar larval brains were dissected in testis buffer (TB: 183 mM KCL, 47 mM NaCl, 10 MM Tris, and 1 mM EDTA, pH 6.8) and brains were fixed for 20 minutes at 25°C in TBF (TB supplemented with 10% formaldehyde, and 0.01% Triton X-100). Brains were then washed twice in PBS for 15 minutes, and twice in PBS Triton X-100 0.1% for 15 minutes. The brains were first incubated for 60 minutes at 25°C in PBSTB (1% BSA), before incubation with secondary antibodies. The samples were observed with a SP5 confocal microscope (Leica) equipped with a 63X 1.4NA objective lens. Images are maximum intensity projections consisting of 4 optical sections acquired at 0.5 µm intervals. The central brain NB number was calculated as the

number of deadpan positive cells and the percentages of euploid, aneuploid and polyploid cells were determined on brain squashed preparation as described before (Caous et al., 2015).

QUANTIFICATION AND STATISTICAL ANALYSES

Quantification of peripheral MTs in fixed NBs during mid anaphase

Z-series were acquired every 0.2 µm using a LSM 880 confocal microscope with Airyscan (Zeiss) for telophase NBs. Images were then processed with the Zen software. Images were analyzed with ImageJ as maximum intensity projections (0.8 µm) consisting of 5 optical (0.2 µm) sections in the plane of the furrow.

Statistical analysis

Differences between datasets were assessed with Prism 7.0a software (GraphPad), either by non-parametric tests (Mann-Whitney) or parametric tests (Unpaired T). Non-significance (ns) threshold was when $P>0.05$. Statistical details can be found in the figure legend, with each "n" representing a distinct neuroblast.

References

ADAMS, R. R., TAVARES, A. A., SALZBERG, A., BELLEN, H. J. & GLOVER, D. M. 1998. pavarotti encodes a kinesin-like protein required to organize the central spindle and contractile ring for cytokinesis. *Genes Dev,* 12**,** 1483-94.

ADRIAANS, I. E., BASANT, A., PONSIOEN, B., GLOTZER, M. & LENS, S. M. A. 2019. PLK1 plays dual roles in centralspindlin regulation during cytokinesis. *J Cell Biol,* 218**,** 1250-1264.

BASANT, A., LEKOMTSEV, S., TSE, Y. C., ZHANG, D., LONGHINI, K. M., PETRONCZKI, M. & GLOTZER, M. 2015. Aurora B kinase promotes cytokinesis by inducing centralspindlin oligomers that associate with the plasma membrane. *Dev Cell,* 33**,** 204-15.

BASTO, R., BRUNK, K., VINADOGROVA, T., PEEL, N., FRANZ, A., KHODJAKOV, A. & RAFF, J. W. 2008. Centrosome amplification can initiate tumorigenesis in flies. *Cell,* 133**,** 1032-42.

BASTO, R., LAU, J., VINOGRADOVA, T., GARDIOL, A., WOODS, C. G., KHODJAKOV, A. & RAFF, J. W. 2006. Flies without centrioles. *Cell,* 125**,** 1375-86.

BERDNIK, D. & KNOBLICH, J. A. 2002. Drosophila Aurora-A is required for centrosome maturation and actin-dependent asymmetric protein localization during mitosis. *Curr Biol,* 12**,** 640-7.

BISCHOF, J., BJORKLUND, M., FURGER, E., SCHERTEL, C., TAIPALE, J. & BASLER, K. 2013. A versatile platform for creating a comprehensive UAS-ORFeome library in Drosophila. *Development,* 140**,** 2434-42.

BRINGMANN, H. & HYMAN, A. A. 2005. A cytokinesis furrow is positioned by two consecutive signals. *Nature,* 436**,** 731-4.

BUSTER, D. W., ZHANG, D. & SHARP, D. J. 2007. Poleward tubulin flux in spindles: regulation and function in mitotic cells. *Mol Biol Cell,* 18**,** 3094-104.

CABERNARD, C., PREHODA, K. E. & DOE, C. Q. 2010. A spindle-independent cleavage furrow positioning pathway. *Nature,* 467**,** 91-4.

CANMAN, J. C., CAMERON, L. A., MADDOX, P. S., STRAIGHT, A., TIRNAUER, J. S., MITCHISON, T. J., FANG, G., KAPOOR, T. M. & SALMON, E. D. 2003. Determining the position of the cell division plane. *Nature,* 424**,** 1074-8.

CAOUS, R., PASCAL, A., ROME, P., RICHARD-PARPAILLON, L., KARESS, R. & GIET, R. 2015. Spindle assembly checkpoint inactivation fails to suppress neuroblast tumour formation in aurA mutant Drosophila. *Nat Commun,* 6**,** 8879.

CLARET, S., JOUETTE, J., BENOIT, B., LEGENT, K. & GUICHET, A. 2014. PI(4,5)P2 produced by the PI4P5K SKTL controls apical size by tethering PAR-3 in Drosophila epithelial cells. *Curr Biol,* 24**,** 1071-9.

CONNELL, M., CABERNARD, C., RICKETSON, D., DOE, C. Q. & PREHODA, K. E. 2011. Asymmetric cortical extension shifts cleavage furrow position in Drosophila neuroblasts. *Mol Biol Cell,* 22**,** 4220-6.

CULLEN, C. F., DEAK, P., GLOVER, D. M. & OHKURA, H. 1999. mini spindles: A gene encoding a conserved microtubule-associated protein required for the integrity of the mitotic spindle in Drosophila. *J Cell Biol,* 146**,** 1005-18.

D'AVINO, P. P., GIANSANTI, M. G. & PETRONCZKI, M. 2015. Cytokinesis in animal cells. *Cold Spring Harb Perspect Biol,* 7**,** a015834.

D'AVINO, P. P., SAVOIAN, M. S. & GLOVER, D. M. 2005. Cleavage furrow formation and ingression during animal cytokinesis: a microtubule legacy. *J Cell Sci,* 118**,** 1549-58.

DIETZL, G., CHEN, D., SCHNORRER, F., SU, K. C., BARINOVA, Y., FELLNER, M., GASSER, B., KINSEY, K., OPPEL, S., SCHEIBLAUER, S., COUTO, A., MARRA,

V., KELEMAN, K. & DICKSON, B. J. 2007. A genome-wide transgenic RNAi library for conditional gene inactivation in Drosophila. *Nature,* 448**,** 151-6.
EDZUKA, T. & GOSHIMA, G. 2019. Drosophila kinesin-8 stabilizes the kinetochore-microtubule interaction. *J Cell Biol,* 218**,** 474-488.
FOE, V. E. & VON DASSOW, G. 2008. Stable and dynamic microtubules coordinately shape the myosin activation zone during cytokinetic furrow formation. *J Cell Biol,* 183**,** 457-70.
FOX, J. C., HOWARD, A. E., CURRIE, J. D., ROGERS, S. L. & SLEP, K. C. 2014. The XMAP215 family drives microtubule polymerization using a structurally diverse TOG array. *Mol Biol Cell,* 25**,** 2375-92.
GALLAUD, E., CAOUS, R., PASCAL, A., BAZILE, F., GAGNE, J. P., HUET, S., POIRIER, G. G., CHRETIEN, D., RICHARD-PARPAILLON, L. & GIET, R. 2014. Ensconsin/Map7 promotes microtubule growth and centrosome separation in Drosophila neural stem cells. *J Cell Biol,* 204**,** 1111-21.
GERVAIS, L., CLARET, S., JANUSCHKE, J., ROTH, S. & GUICHET, A. 2008. PIP5K-dependent production of PIP2 sustains microtubule organization to establish polarized transport in the Drosophila oocyte. *Development,* 135**,** 3829-38.
GLOTZER, M. 2017. Cytokinesis in Metazoa and Fungi. *Cold Spring Harb Perspect Biol,* 9.
GOSHIMA, G. & VALE, R. D. 2005. Cell cycle-dependent dynamics and regulation of mitotic kinesins in Drosophila S2 cells. *Mol Biol Cell,* 16**,** 3896-907.
GOSHIMA, G., WOLLMAN, R., STUURMAN, N., SCHOLEY, J. M. & VALE, R. D. 2005. Length control of the metaphase spindle. *Curr Biol,* 15**,** 1979-88.
HYMAN, A., DRECHSEL, D., KELLOGG, D., SALSER, S., SAWIN, K., STEFFEN, P., WORDEMAN, L. & MITCHISON, T. 1991. Preparation of modified tubulins. *Methods Enzymol,* 196**,** 478-85.
INOUE, Y. H., SAVOIAN, M. S., SUZUKI, T., MATHE, E., YAMAMOTO, M. T. & GLOVER, D. M. 2004. Mutations in orbit/mast reveal that the central spindle is comprised of two microtubule populations, those that initiate cleavage and those that propagate furrow ingression. *J Cell Biol,* 166**,** 49-60.
JANUSCHKE, J. & GONZALEZ, C. 2008. Drosophila asymmetric division, polarity and cancer. *Oncogene,* 27**,** 6994-7002.
JORDAN, P. & KARESS, R. 1997. Myosin light chain-activating phosphorylation sites are required for oogenesis in Drosophila. *J Cell Biol,* 139**,** 1805-19.
KALTSCHMIDT, J. A., DAVIDSON, C. M., BROWN, N. H. & BRAND, A. H. 2000. Rotation and asymmetry of the mitotic spindle direct asymmetric cell division in the developing central nervous system. *Nat Cell Biol,* 2**,** 7-12.
KNOBLICH, J. A. 2010. Asymmetric cell division: recent developments and their implications for tumour biology. *Nat Rev Mol Cell Biol,* 11**,** 849-60.
KOTYNKOVA, K., SU, K. C., WEST, S. C. & PETRONCZKI, M. 2016. Plasma Membrane Association but Not Midzone Recruitment of RhoGEF ECT2 Is Essential for Cytokinesis. *Cell Rep,* 17**,** 2672-2686.
LAYCOCK, J. E., SAVOIAN, M. S. & GLOVER, D. M. 2006. Antagonistic activities of Klp10A and Orbit regulate spindle length, bipolarity and function in vivo. *J Cell Sci,* 119**,** 2354-61.
LEE, M. J., GERGELY, F., JEFFERS, K., PEAK-CHEW, S. Y. & RAFF, J. W. 2001. Msps/XMAP215 interacts with the centrosomal protein D-TACC to regulate microtubule behaviour. *Nat Cell Biol,* 3**,** 643-9.
MATHIEU, J., CAUVIN, C., MOCH, C., RADFORD, S. J., SAMPAIO, P., PERDIGOTO, C. N., SCHWEISGUTH, F., BARDIN, A. J., SUNKEL, C. E., MCKIM, K., ECHARD, A. & HUYNH, J. R. 2013. Aurora B and cyclin B have opposite effects on

the timing of cytokinesis abscission in Drosophila germ cells and in vertebrate somatic cells. *Dev Cell,* 26**,** 250-65.
MENNELLA, V., ROGERS, G. C., ROGERS, S. L., BUSTER, D. W., VALE, R. D. & SHARP, D. J. 2005. Functionally distinct kinesin-13 family members cooperate to regulate microtubule dynamics during interphase. *Nat Cell Biol,* 7**,** 235-45.
METIVIER, M., MONROY, B. Y., GALLAUD, E., CAOUS, R., PASCAL, A., RICHARD-PARPAILLON, L., GUICHET, A., ORI-MCKENNEY, K. M. & GIET, R. 2019. Dual control of Kinesin-1 recruitment to microtubules by Ensconsin in Drosophila neuroblasts and oocytes. *Development,* 146.
MINESTRINI, G., HARLEY, A. S. & GLOVER, D. M. 2003. Localization of Pavarotti-KLP in living Drosophila embryos suggests roles in reorganizing the cortical cytoskeleton during the mitotic cycle. *Mol Biol Cell,* 14**,** 4028-38.
MINESTRINI, G., MATHE, E. & GLOVER, D. M. 2002. Domains of the Pavarotti kinesin-like protein that direct its subcellular distribution: effects of mislocalisation on the tubulin and actin cytoskeleton during Drosophila oogenesis. *J Cell Sci,* 115**,** 725-36.
MISHIMA, M. 2016. Centralspindlin in Rappaport's cleavage signaling. *Semin Cell Dev Biol,* 53**,** 45-56.
MORALES-MULIA, S. & SCHOLEY, J. M. 2005. Spindle Pole Organization in Drosophila S2 Cells by Dynein, Abnormal Spindle Protein (Asp), and KLP10A. *Mol Biol Cell,* 16**,** 3176-86.
MURTHY, K. & WADSWORTH, P. 2008. Dual role for microtubules in regulating cortical contractility during cytokinesis. *J Cell Sci,* 121**,** 2350-9.
RADFORD, S. J., HARRISON, A. M. & MCKIM, K. S. 2012. Microtubule-depolymerizing kinesin KLP10A restricts the length of the acentrosomal meiotic spindle in Drosophila females. *Genetics,* 192**,** 431-40.
RAMIREZ-RIOS, S., SERRE, L., STOPPIN-MELLET, V., PREZEL, E., VINIT, A., COURRIOL, E., FOUREST-LIEUVIN, A., DELAROCHE, J., DENARIER, E. & ARNAL, I. 2017. A TIRF microscopy assay to decode how tau regulates EB's tracking at microtubule ends. *Methods Cell Biol,* 141**,** 179-197.
RAPPAPORT, R. 1971. Cytokinesis in animal cells. *Int Rev Cytol,* 31**,** 169-213.
REBER, S. B., BAUMGART, J., WIDLUND, P. O., POZNIAKOVSKY, A., HOWARD, J., HYMAN, A. A. & JULICHER, F. 2013. XMAP215 activity sets spindle length by controlling the total mass of spindle microtubules. *Nat Cell Biol,* 15**,** 1116-22.
REBOLLO, E., SAMPAIO, P., JANUSCHKE, J., LLAMAZARES, S., VARMARK, H. & GONZALEZ, C. 2007. Functionally unequal centrosomes drive spindle orientation in asymmetrically dividing Drosophila neural stem cells. *Dev Cell,* 12**,** 467-74.
ROTH, M., ROUBINET, C., IFFLANDER, N., FERRAND, A. & CABERNARD, C. 2015. Asymmetrically dividing Drosophila neuroblasts utilize two spatially and temporally independent cytokinesis pathways. *Nat Commun,* 6**,** 6551.
ROUBINET, C., TSANKOVA, A., PHAM, T. T., MONNARD, A., CAUSSINUS, E., AFFOLTER, M. & CABERNARD, C. 2017. Spatio-temporally separated cortical flows and spindle geometry establish physical asymmetry in fly neural stem cells. *Nat Commun,* 8**,** 1383.
ROYOU, A., SULLIVAN, W. & KARESS, R. 2002. Cortical recruitment of nonmuscle myosin II in early syncytial Drosophila embryos: its role in nuclear axial expansion and its regulation by Cdc2 activity. *J Cell Biol,* 158**,** 127-37.
RUEDEN, C. T., SCHINDELIN, J., HINER, M. C., DEZONIA, B. E., WALTER, A. E., ARENA, E. T. & ELICEIRI, K. W. 2017. ImageJ2: ImageJ for the next generation of scientific image data. *BMC Bioinformatics,* 18**,** 529.

RUSAN, N. M. & PEIFER, M. 2007. A role for a novel centrosome cycle in asymmetric cell division. *J Cell Biol,* 177**,** 13-20.

SHANNON, K. B., CANMAN, J. C., BEN MOREE, C., TIRNAUER, J. S. & SALMON, E. D. 2005. Taxol-stabilized microtubules can position the cytokinetic furrow in mammalian cells. *Mol Biol Cell,* 16**,** 4423-36.

STRICKLAND, L. I., DONNELLY, E. J. & BURGESS, D. R. 2005. Induction of cytokinesis is independent of precisely regulated microtubule dynamics. *Mol Biol Cell,* 16**,** 4485-94.

SUNG, H. H., TELLEY, I. A., PAPADAKI, P., EPHRUSSI, A., SURREY, T. & RORTH, P. 2008. Drosophila ensconsin promotes productive recruitment of Kinesin-1 to microtubules. *Dev Cell,* 15**,** 866-76.

TSANKOVA, A., PHAM, T. T., GARCIA, D. S., OTTE, F. & CABERNARD, C. 2017. Cell Polarity Regulates Biased Myosin Activity and Dynamics during Asymmetric Cell Division via Drosophila Rho Kinase and Protein Kinase N. *Dev Cell,* 42**,** 143-155 e5.

VALE, R. D., SPUDICH, J. A. & GRIFFIS, E. R. 2009. Dynamics of myosin, microtubules, and Kinesin-6 at the cortex during cytokinesis in Drosophila S2 cells. *J Cell Biol,* 186**,** 727-38.

VERMA, V. & MARESCA, T. J. 2019. Microtubule plus-ends act as physical signaling hubs to activate RhoA during cytokinesis. *Elife,* 8.

VERNI, F., SOMMA, M. P., GUNSALUS, K. C., BONACCORSI, S., BELLONI, G., GOLDBERG, M. L. & GATTI, M. 2004. Feo, the Drosophila homolog of PRC1, is required for central-spindle formation and cytokinesis. *Curr Biol,* 14**,** 1569-75.

VON DASSOW, G. 2009. Concurrent cues for cytokinetic furrow induction in animal cells. *Trends Cell Biol,* 19**,** 165-73.

WANG, H., BRUST-MASCHER, I. & SCHOLEY, J. M. 2015. The microtubule cross-linker Feo controls the midzone stability, motor composition, and elongation of the anaphase B spindle in Drosophila embryos. *Mol Biol Cell,* 26**,** 1452-62.

WIDMANN, T. J. & DAHMANN, C. 2009. Dpp signaling promotes the cuboidal-to-columnar shape transition of Drosophila wing disc epithelia by regulating Rho1. *J Cell Sci,* 122**,** 1362-73.

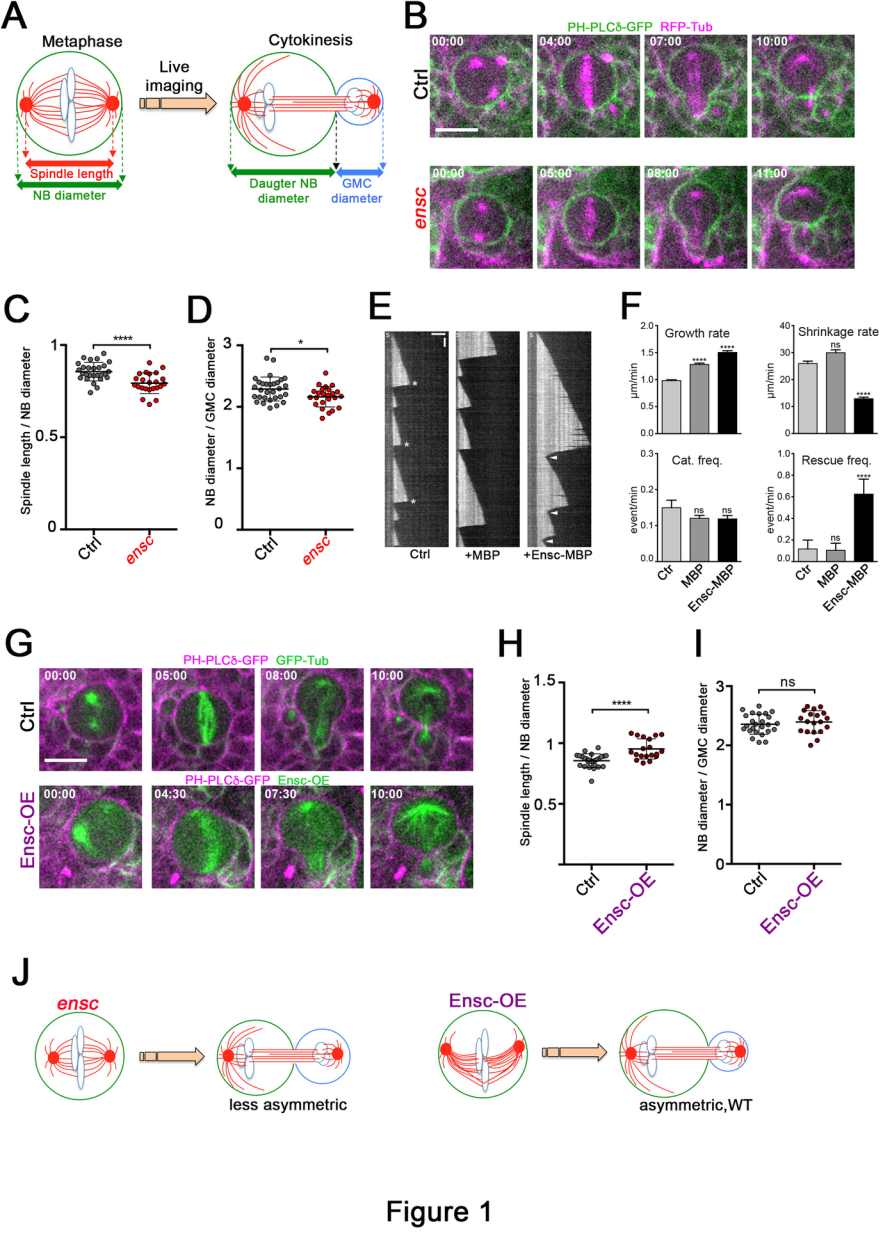
A
Metaphase
Live imaging
Cytokinesis
Spindle length
NB diameter
Daugter NB diameter
GMC diameter
B
PH-PLCδ-GFP RFP-Tub
Ctrl
ensc
00:00
04:00
07:00
10:00
05:00
08:00
11:00
C
Spindle length / NB diameter
****
Ctrl
ensc
D
NB diameter / GMC diameter
*
E
Ctrl
+MBP
+Ensc-MBP
F
Growth rate
μm/min
Shrinkage rate
ns
Cat. freq.
event/min
Rescue freq.
Ctr
MBP
Ensc-MBP
G
PH-PLCδ-GFP GFP-Tub
PH-PLCδ-GFP Ensc-OE
Ensc-OE
H
I
NB diameter / GMC diameter
J
less asymmetric
Ensc-OE
asymmetric,WT

Figure 1

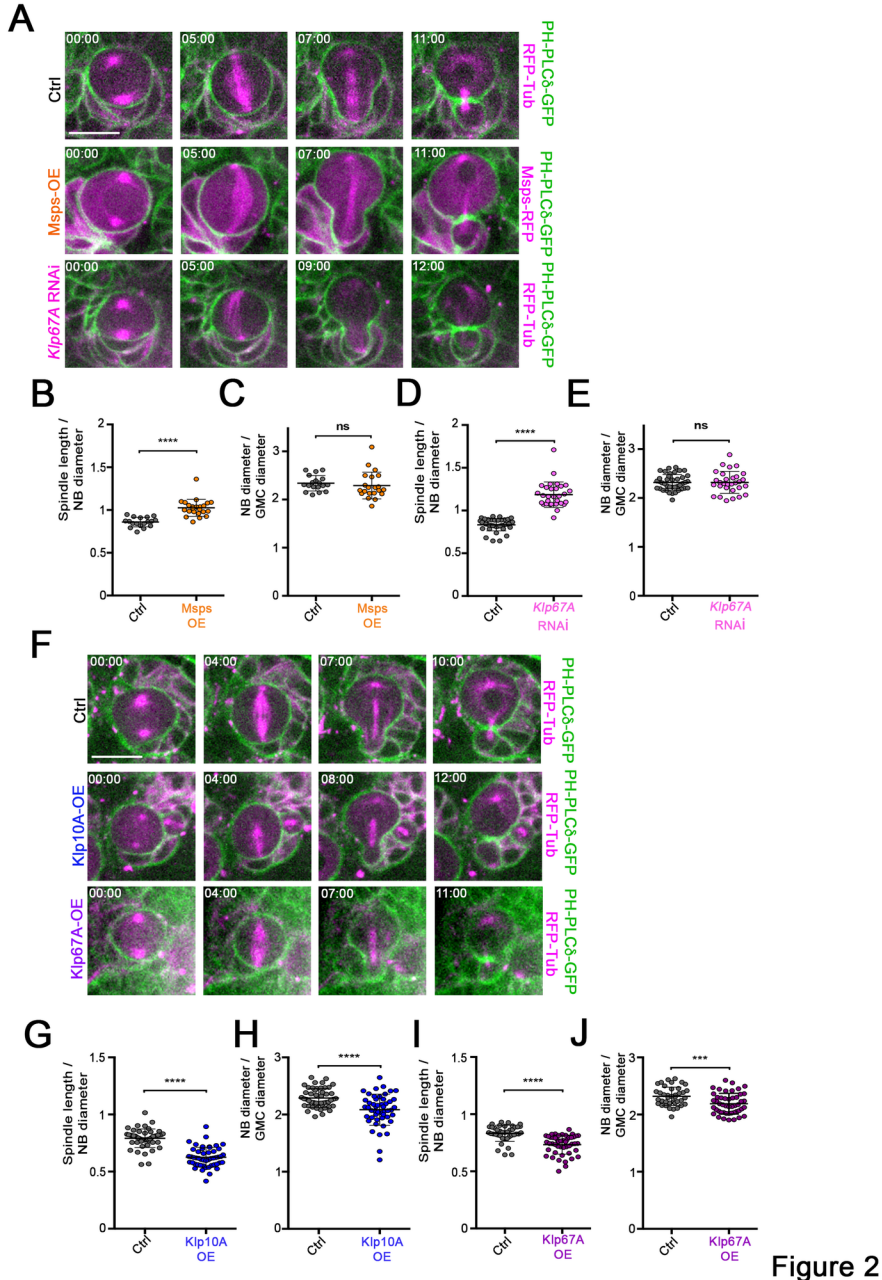
A
Ctrl
Msps-OE
Klp67A RNAi
00:00
05:00
07:00
09:00
11:00
12:00
PH-PLCδ-GFP
RFP-Tub
Msps-RFP
B
C
D
E
Spindle length / NB diameter
NB diameter / GMC diameter
****
ns
Ctrl
Msps OE
Klp67A RNAi
F
04:00
08:00
10:00
Klp10A-OE
Klp67A-OE
G
H
I
J
***
Klp10A OE
Klp67A OE

Figure 2

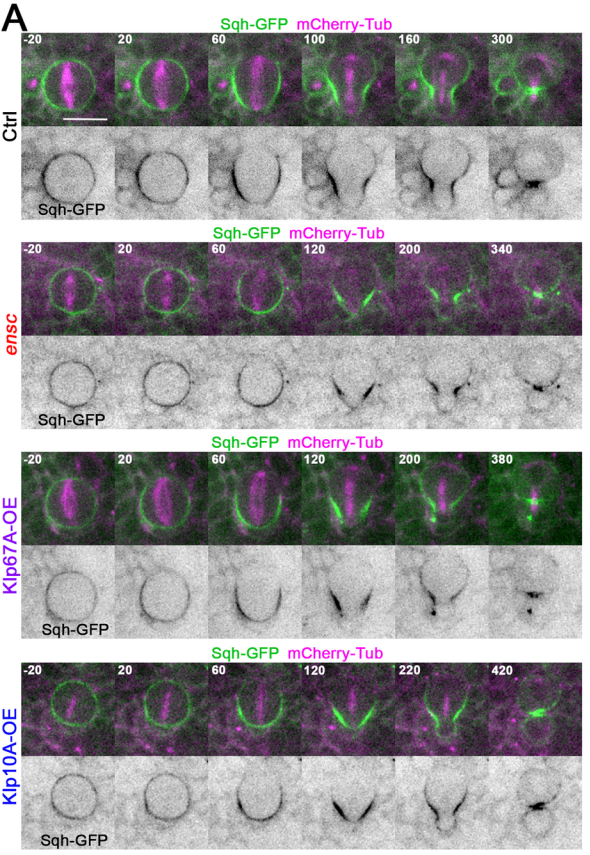
A
Sqh-GFP mCherry-Tub
-20
20
60
100
160
300
Ctrl
Sqh-GFP
Sqh-GFP mCherry-Tub
-20
20
60
120
200
340
ensc
Sqh-GFP
Sqh-GFP mCherry-Tub
-20
20
60
120
200
380
Klp67A-OE
Sqh-GFP
Sqh-GFP mCherry-Tub
-20
20
60
120
220
420
Klp10A-OE
Sqh-GFP
B
Initial
Shift
Final
C
Normalized furrow shift
-0.1
0.0
0.1
0.2
0.3
****
***
*
Ctrl
ensc
Klp67A-OE
Klp10A-OE
D
Furrow
Width
E
Normalized furrow width
0.6
0.4
0.2
0
****
*
***
Ctrl
ensc
Klp67A-OE
Klp10A-OE

Figure 3

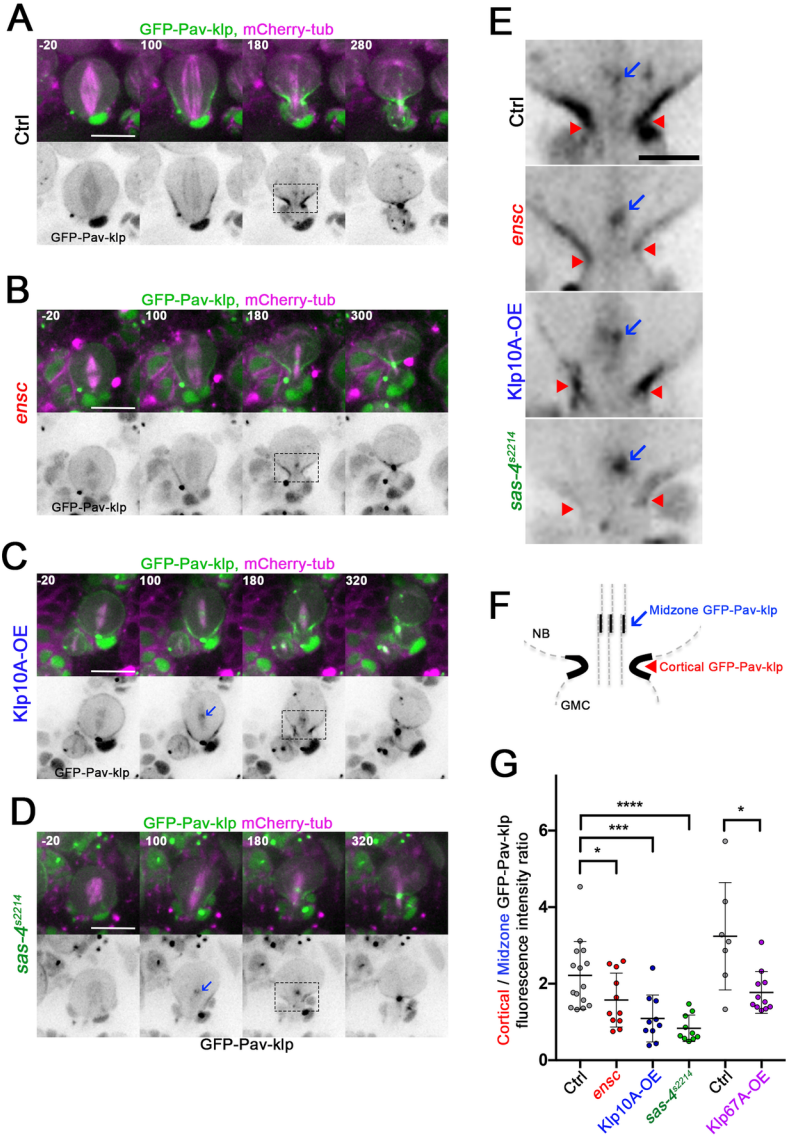
A
GFP-Pav-klp, mCherry-tub
-20
100
180
280
Ctrl
GFP-Pav-klp
B
GFP-Pav-klp, mCherry-tub
-20
100
180
300
ensc
GFP-Pav-klp
C
GFP-Pav-klp, mCherry-tub
-20
100
180
320
Klp10A-OE
GFP-Pav-klp
D
GFP-Pav-klp mCherry-tub
-20
100
180
320
sas-4s2214
GFP-Pav-klp
E
Ctrl
ensc
Klp10A-OE
sas-4s2214
F
NB
Midzone GFP-Pav-klp
Cortical GFP-Pav-klp
GMC
G
Cortical / Midzone GFP-Pav-klp fluorescence intensity ratio
****
***
*
*
0
2
4
6
Ctrl
ensc
Klp10A-OE
sas-4s2214
Ctrl
Klp67A-OE

Figure 4

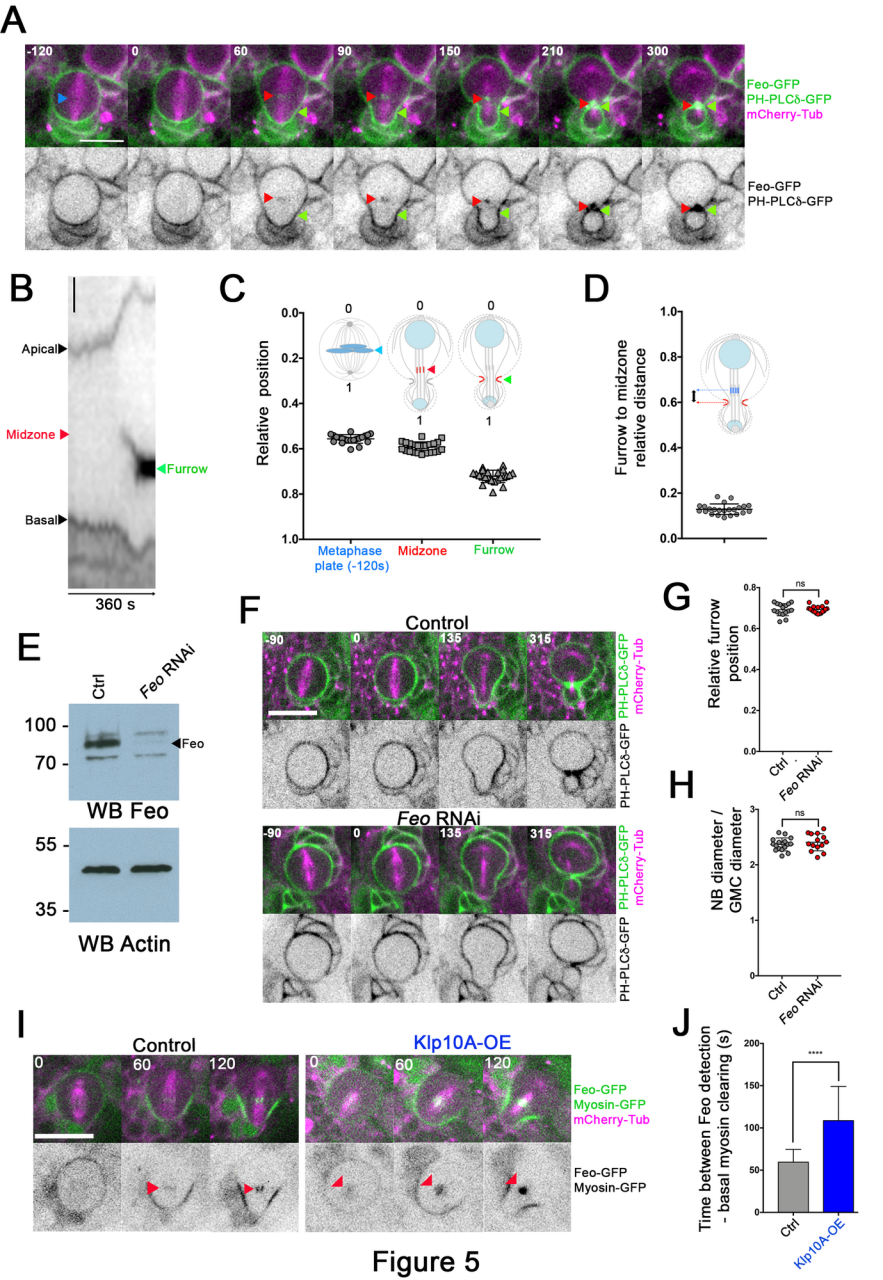
A
-120
0
60
90
150
210
300
Feo-GFP
PH-PLCδ-GFP
mCherry-Tub
Feo-GFP
PH-PLCδ-GFP
B
Apical
Midzone
Furrow
Basal
360 s
C
Relative position
Metaphase plate (-120s)
Midzone
Furrow
D
Furrow to midzone relative distance
E
Ctrl
Feo RNAi
100
70
Feo
WB Feo
55
35
WB Actin
F
Control
-90
0
135
315
PH-PLCδ-GFP
mCherry-Tub
Feo RNAi
G
Relative furrow position
ns
Ctrl
Feo RNAi
H
NB diameter / GMC diameter
ns
Ctrl
Feo RNAi
I
Control
Klp10A-OE
0
60
120
Feo-GFP
Myosin-GFP
mCherry-Tub
J
Time between Feo detection - basal myosin clearing (s)
****
Ctrl
Klp10A-OE

Figure 5

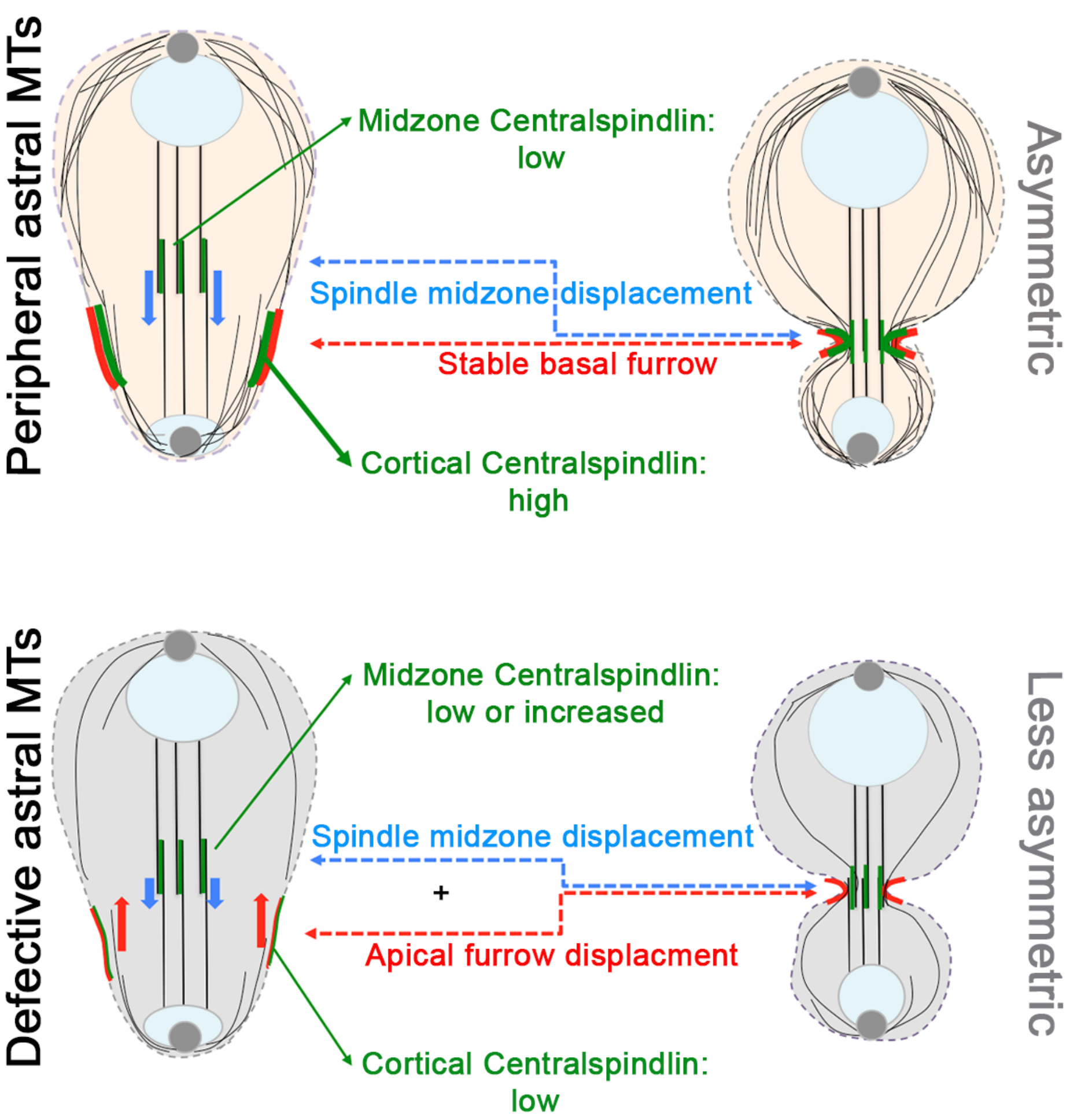
Peripheral astral MTs
Midzone Centralspindlin:
low
Spindle midzone displacement
Stable basal furrow
Cortical Centralspindlin:
high
Asymmetric
Defective astral MTs
Midzone Centralspindlin:
low or increased
Spindle midzone displacement
+
Apical furrow displacment
Cortical Centralspindlin:
low
Less asymmetric